BJR

https://doi.org/10.1259/bjr.20220512

Received: 17 May 2022 | Revised: 11 October 2022 | Accepted: 19 October 2022 | Published online: 17 November 2022

Cite this article as:
Wei H, Shao Z, Fu F, Yu X, Wu Y, Bai Y, et al. Value of multimodal MRI radiomics and machine learning in predicting staging liver fibrosis and grading inflammatory activity. *Br J Radiol* (2023) 10.1259/bjr.20220512.

FULL PAPER

Value of multimodal MRI radiomics and machine learning in predicting staging liver fibrosis and grading inflammatory activity

[1]HUANHUAN WEI, [2]ZEHUA SHAO, [3]FANGFANG FU, [3]XUAN YU, [3]YAPING WU, [3]YAN BAI, [3]WEI WEI, [1]NAN MENG, [4]KEWEI LIU, [5]HUI HAN and [1,3]MEIYUN WANG

[1]Academy of Medical Sciences, the People's Hospital of Zhengzhou University, Zhengzhou, Henan, China
[2]Heart Center of Zhengzhou University People's Hospital, Henan Provincial People's Hospital, Zhengzhou, Henan Province, China
[3]Department of Medical Imaging, Henan Provincial People's Hospital & the People's Hospital of Zhengzhou University, Zhengzhou, Henan, China
[4]The First People's Hospital of Zhoukou, Zhoukou, Henan, China
[5]Biomedical Imaging Research Institute, Cedars-Sinai Medical Center, Los Angeles, CA, USA

Address correspondence to: MD Meiyun Wang
E-mail: *mywang@zzu.edu.cn*

Huanhuan Wei, Zehua Shao, Fangfang Fu and Xuan Yu have contributed equally to this study and should be considered as co-first authors.

Objective: To evaluate the value of radiomics models created based on non-contrast enhanced T_1 weighted (T_1W) and T_2W fat-saturated (T_2WFS) images for staging hepatic fibrosis (HF) and grading inflammatory activity.
Methods and materials: Data of 280 patients with pathologically confirmed HF and 48 healthy volunteers were included. The participants were divided into the training set and the test set at the proportion of 4:1 by the random seed method. We used the Pyradiomics software to extract radiomics features, and then use the least absolute shrinkage and selection operator to select the optimal subset. Finally, we used the stochastic gradient descent classifier to build the prediction models. DeLong test was used to compare the diagnostic performance of the models. Receiver operating characteristics was used to evaluate the prediction ability of the models.
Results: The diagnostic efficiency of the models based on T_1W & T_2WFS images were the highest (all $p < 0.05$). When discriminating significant fibrosis (≥ F2), there were significant differences in the AUCs between the machine learning models based on T_1W and T_2WFS images ($p < 0.05$), but there were no significant differences in area under the receiver operating characteristic curves between the two models in other groups (all $p > 0.05$).
Conclusion: The radiomics models built on T_1W and T_2WFS images are effective in assessing HF and inflammatory activity.
Advances in knowledge: Based on conventional MR sequences that are readily available in the clinic, namely unenhanced T_1W and T_2W images. Radiomics can be used for diagnosis and differential diagnosis of liver fibrosis staging and inflammatory activity grading.

INTRODUCTION

Hepatic fibrosis (HF) is a pathological repairing process response to liver damage caused by chronic liver disease (CLD), which may be caused by various reasons (including virus, alcohol, drug damage, autoimmune, cholestasis and metabolic diseases), accompanied by abnormal deposition of connective tissue in the liver. Most clinical studies have shown that non-advanced HF can be reversed by clinical intervention.[1] However, CLD without effective treatment can eventually develop cirrhosis or liver failure, and even increases the risk of primary malignant liver tumors, especially hepatocellular carcinoma.[2] Therefore, accurate early diagnosis of HF is important for the treatment selection and prognosis of CLD. The current gold-standard for the diagnosis of HF is still liver puncture biopsy, however, this technique is invasive and difficult to be accepted by patients. Besides, the accuracy of the pathological results is also affected by subjective and objective factors.[3] Moreover, the risk caused by liver biopsy may lead to death in 0.018% of patients.[4] Accordingly, a non-invasive method for accurate diagnosis and staging of HF is highly needed.

The evaluation of liver disease severity by non-invasive liver imaging has become a major hot topic in recent years.[5] Many researchers have evaluated HF using functional MRI such as diffusion-weighted imaging (DWI) with the apparent diffusion coefficient (ADC), which is based on the Brownian motion of water molecules in biological tissue, and they find that ADC value has a certain correlation with the degree of HF.[6,7] However, the measurement of liver ADC may be affected by many factors,[8] including b value, steatosis, iron content, etc. All these factors may have significant influences on repeatability and stability of the results. Magnetic resonance elastography (MRE) has also been used to study the fibrosis stages, based on the principle of measuring liver hardness.[9,10] Although MRE is effective in evaluating HF, it is expensive and requires additional equipment support. Moreover, the iron overload will reduce the signal-to-noise ratio of the images and lead to the inaccuracy of the MRE.[11] Therefore, a more practical and effective detecting method holds great promise in the future.

Dutch scholars Lambin et al[12] proposed the concept of radiomics in 2012. Up to now, radiomics analysis is the high-throughput mining of quantitative image features from medical images such as CT, MRI or PET, including statistical features, morphological features and texture features, with subsequent analysis to apply to clinical decision-support systems. Radiomics methods analyze medical images through high-throughput feature mining and extraction methods, which can realize the quantitative description of medical images, and solve the problem that a large number of image features are easily ignored by the naked eye.[13] Although there have been many studies on HF staging by radiomics methods, to our knowledge, few studies have established the radiomics models using multimodal MR images to stage HF and grade inflammatory activity simultaneously. We hypothesized that models with radiomics features extracted from non-contrast-enhanced T_1 weighted (T_1W) and T_2W fat-saturated (T_2WFS) images could comprehensively assess images features associated with HF and inflammatory activity. Therefore, this study aims to develop and validate radiomics models in the evaluation of HF and inflammatory activity by using non-contrast-enhanced T_1W and T_2WFS images.

METHODS AND MATERIALS

Study population

This retrospective study was approved by the institutional review board of the ethics committee of the Zhengzhou University People's Hospital & Henan Provincial People's Hospital. Between December 2018 and May 2021, 308 patients with CLD were recruited for a routine hepatic magnetic resonance (MR) sequence. Inclusion criteria: (a) age >18 years. (b) All patients were confirmed pathologically by liver biopsy and met the diagnostic criteria of HF. MR imaging was performed before liver biopsy, and the interval between the two tests was less than 1 month. (c) The clinical and pathological data of the included cases were complete. Exclusion criteria: (a) MR images with bad quality due to large artifacts. (b) Severe diffuse lesions in the liver, as tumors or multiple cysts, etc. According to the exclusion and inclusion criteria, 28 patients were excluded for the following reasons: 15 cases had surgery on the right lobe of the liver, 7 cases had poor images with artifacts, and 6 patients had multiple intrahepatic space-occupying lesions. A total of 280 patients were enrolled (mean age 41 years; aged between 18 and 78; 170 males and 110 females), including 205 cases of hepatitis B, 35 cases of hepatitis C, 16 cases of autoimmune hepatitis, 12 cases of non-alcoholic fatty liver disease, and 12 cases of drug-induced hepatitis (Table 1). Meanwhile, the control group recruited 48 healthy volunteers (mean age 39 years old; age between 22 and 75 years old). They had no liver biopsy or surgical liver biopsy for pathology, nor did they have a history of liver-related diseases and evidence. In this study, the liver fibrosis stage of these volunteers was defined as F0, and the grade of inflammatory activity was classified as A0 (Figure 1). Routine liver MRI was performed for all healthy subjects.

Table 1. Characteristics of the study population.

Characteristic	Patients (n = 280)	Healthy volunteers (n = 48)
Sex (males)	170 (86.3%)	27 (13.7%)
Mean age ± SD	40.2 ± 8.5	41.5 ± 10.2
Etiology of liver disease (n = 280)		
HBV	205	
HCV	35	
Autoimmune hepatitis	16	
Non-alcoholic fatty liver disease	12	
Drug-induced hepatitis	12	
Fibrosis score (METAVIR)		
F0/A0	48/48	48
F1/A1	53/73	
F2/A2	92/124	
F3/A3	73/83	
F4	62	

Histopathological analysis

Histology of the right lobe and/or right posterior lobe of the liver was obtained by a liver pathologist (with 11 years of experience) through percutaneous liver biopsy (16G or 18G needles). The liver pathologist was blind to the imaging data of all patients and used the METAVIR scoring system[14] to provide consistent scores. The degree of fibrosis was staged as follows: F0 = with no fibrosis, F1 = portal fibrosis without septa, F2 = portal fibrosis with rare septa, F3 = numerous septa without cirrhosis, and F4 = cirrhosis. The inflammatory activity was graded as follows: A0 = no activity, A1 = mild activity, A2 = moderate activity, and A3 = severe activity.

MRI examinations

All participants were performed MRI by using Discovery MR750 (Discovery MR750; GE Medical System, Milwaukee, WI) with eight-channel phased array coils (GE Medical System, Milwaukee, WI) or Discovery MR750plus tests. The parameters

Figure 1. Patients selection flow chart.

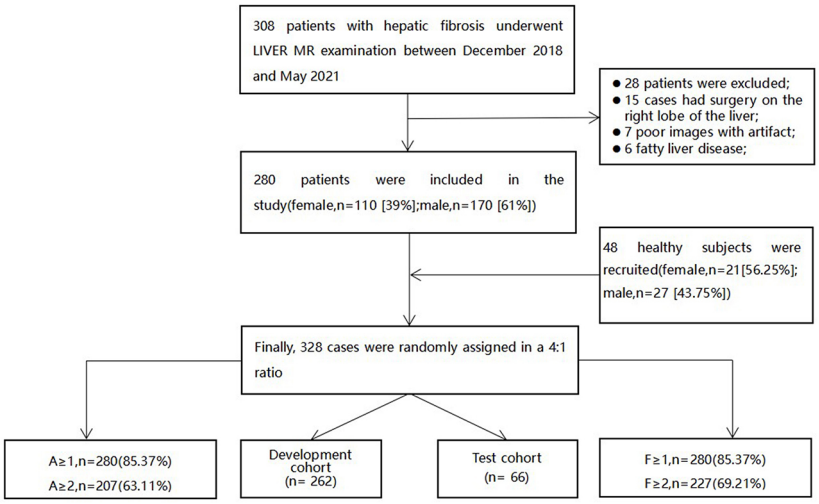

of both inspection equipment were consistent as shown in the table below (Table 2). All participants fasted for at least 6 h before MR examination. They received conventional liver MRI sequences, including axial T_1W fast spoiled gradient recalled and axial T_2WFS fast spin echo sequences (fat suppression).

Imaging analysis

The acquired images were transmitted to the AW4.6 workstation (Advantage workstation 4.6; General Electric Medical System) for processing and analyzing by a radiologist (6 years of abdominal MRI diagnostic experience) who was unaware of the clinical evaluation and pathological classification. Application of ITK-SNAP software (http://www.itk-snap.org) manually delineated the region of interest (ROI) on T_1W and T_2WFS images, respectively, to complete the segmentation of lesion images. The radiologist drew the ROI at the right lobe of the T_2WFS images, drawing three consecutive axial images through the center of the liver at the level of the right portal vein (A similar approach has previously been used in staging HF).[15] In order to maintain the consistency of each square ROI, the assessor loaded ROIs with a length of 25 pixels on each side-from a file containing a standard size ROI box, and copied the ROI to the T_1W images of the same slice. The ROIs were placed in the liver avoiding the large liver blood vessels, bile ducts and artifacts (Figure 2).

Radiomics features extraction and selection

Radiomics analysis was performed with uAI Research Portal (United Imaging Intelligence, China), which is a clinical research platform and implemented by Python programming language (v. 3.7.3, https://www.python.org). Firstly, we pre-processed the T_1W and T_2WFS images of all participants with image brightness normalization using the Z-score method. Secondly, the image features were calculated using the image data processed by PyRadiomics (https://pyradiomics.readthedocs.io/en/latest/index.html). Finally, a total of 2600 radiomics features were calculated from the original images and the derived images generated by the filter, including 450 first-level statistical features, 350 morphological features and 1800 texture features. The T_1W & T_2WFS features set was generated by means of features stitching.

The data set was randomly divided into training and test cohorts at a ratio of 4:1, the training cohort was used for features selection and models construction, and the test cohort was used for models' evaluation. We used variance threshold method to remove features with low variance, and subsequently sieved for significant features by F-test ($p < 0.05$). We further performed the least absolute shrinkage and selection operator to eliminate features with high collinearity and avoid overfitting. Finally, a total of 30 features (8 statistical, 12 structural, and 10 morphological features) were yielded for the following analysis. For the features selected by the above method, scikit-Learn (https://scikit-learn.org/stable/) was used for data pre-processing, features reduction and models training. Three classification models were obtained for each group according to T_1W, T_2WFS and T_1W&T_2WFS images. The assessor plotted the receiver operating characteristics (ROC) curve of the models, calculated the AUC value and used the DeLong test to evaluate whether there was a significant difference between those models.[16] For the model with the highest AUC value, the Youden index was used to determine the fibrosis score threshold, and the sensitivity and specificity of the model were calculated.

Model construction

The selected features were modeled using the stochastic gradient descent (SGD) classifier, and the feature sample size estimation was based on a rule of thumb.[17] 5–10 highly correlated features were extracted from T_1W, T_2WFS and T_1W&T_2WFS images, including statistical features, texture features, and morphological features, to build models for predicting HF stages (including $F \geq 1$, $F \geq 2$) and inflammatory activity grades (including $A \geq 1$, $A \geq 2$), respectively. The prediction ability of the models was validated using an internally validated method. AUC was used to quantify the power of the prediction models for predicting the stage of HF and the grade of inflammatory activity. The corresponding sensitivity and specificity were calculated as well.

Statistical analysis

SPSS 26.0 software (SPSS, Chicago, IL) was used for the statistical analysis of data. The data following the normal distribution

Table 2. Magnetic resonance scanning sequence and imaging parameters

Magnetic resonance sequence	TR	TE	Slick	Layer spacing	NEX	Flip angle	Bandwidth	Matrix	FOV	Resolution ratio	
T_1W	72 ms	2.1 ms	5 mm	2.5 mm	1	12	200 KHz	512 × 512	380 mm	0.74 × 0.74	
T_2WFS	4286 ms	76 ms	5 mm	2.5 mm	1.5	80	83.33 KHz	512 × 512	380 mm	0.74 × 0.74	

FOV, field of view; NEX, number of excitations; TE, echo time; TR, repetition time.

Figure 2. ROI delineation diagram of MR images. The above two pictures (A, B) show the normal MR images of a 44-year-old female. (A) T_1W sequence; (B) T_2WFS sequence; The two images below (C, D) show a 45-year-old male patient with chronic viral hepatitis B with fibrosis Stage 2 and inflammatory activity Grade 2; (C) T_1W sequence; (D) T_2WFS sequence; The red squares are the ROI. ROI, region of interest.

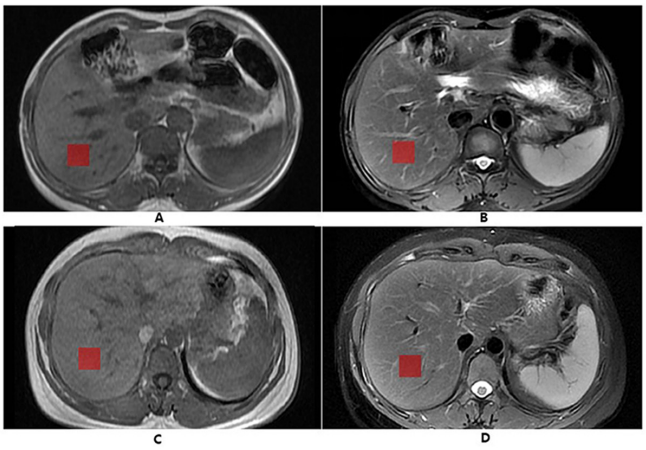

were expressed as mean ± SD. Count data were showed as n (%). The DeLong test was used to compare the diagnostic power of each machine learning model between fibrosis stages ≤ F0 and ≥ F1, and stages ≤ F1 and ≥ F2. In addition, the DeLong test was used to compare the diagnostic power of each machine learning model between inflammatory activity grades ≤ A0 and ≥ A1, and grades ≤ A1 and ≥ A2. ROC curves were calculated for all parameters to assess the AUC and to determine the best model. Results with a p-value < 0.05 were considered significantly different.

RESULTS

Patient characteristics

The characteristics of demographic variables, the stages of HF and grades of necrotizing inflammatory activity analysis were summarized in Table 1. HF stages and inflammatory activity grades were histologically quantified by liver biopsy in 280 patients. 48 healthy liver volunteers were considered to be fibrosis Stage 0 and inflammatory activity Grade 0. The fibrosis stages distribution were as follows: $F \geq 1$, $n = 280$ (85.37%); $F \geq 2$, $n = 227$ (69.21%); the inflammatory activity grades distribution were as follows: $A \geq 1$, $n = 280$ (85.37%); $A \geq 2$, $n = 207$ (63.11%) (Figure 1, Table 1).

In Figure 2, A and B were T_1W and T_2WFS images of normal volunteers, respectively; C and D were T_1W and T_1WFS images of fibrous patients with fibrosis Stage 2 and inflammatory activity Grade 2, respectively.

Effectiveness of radiomics labels in predicting staging of HF

In the test set, when differentiating $F \geq 1$, ROC analyses of the constructed models based on the radiomics features of T_1W, T_2WFS and T_1W&T_2WFS images showed that the AUCs of three models were 0.844, 0.857 and 0.932, respectively, among them the T_1W&T_2WFS model had the best diagnostic efficacy (all p

Figure 3. ROC curves of the models for predicting the stage of liver fibrosis and the grade of inflammatory activity

(a), (b) ROC curves for models built based on radiomics features of T_1W, T_2WFS, and T_1W&T_2WFS images for discriminating fibrosis stage $F \geq 1$and $F \geq 2$; (c), (d) ROC curves for models built based on radiomics features of T_1W, T_2WFS, and T_1W&T_2WFS images for discriminating inflammatory activity grade $A \geq 1$and $A \geq 2$. ROC, receiver operating characteristic.

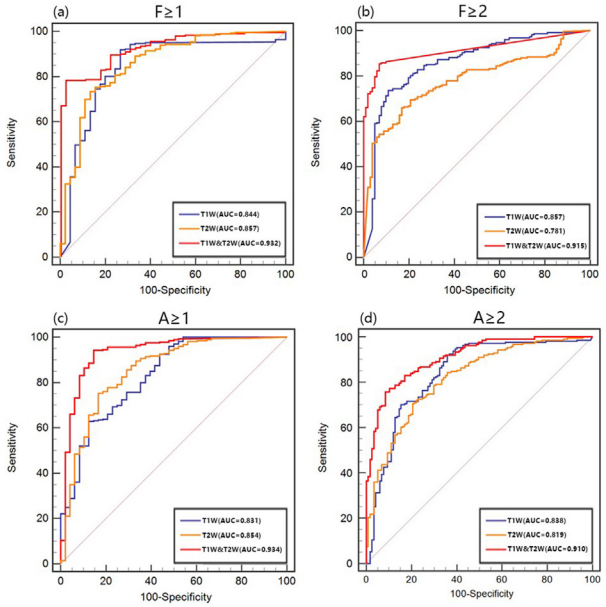

< 0.05), and there was no significant difference between T_1W model and T_2WFS model ($p > 0.05$). When differentiating $F \geq 2$, the AUCs of T_1W, T_2WFS and T_1W&T_2WFS model were 0.857, 0.781 and 0.915, respectively. Among them, the T_1W&T_2WFS model had the best diagnostic efficacy (all $p < 0.05$), followed by T_1W model (Figure 3,Table 3).

Effectiveness of radiomics labels in predicting staging of grading of inflammatory activity

In the test set, ROC analyses of the constructed models based on the radiomics features of T_1W, T_2WFS and T_1W&T_2WFS images, when differentiating $A \geq 1$, showed that the AUCs of three models were 0.831, 0.854 and 0.934, respectively; when differentiating $A \geq 2$, the AUCs of three models were 0.838, 0.819 and 0.910, respectively. The diagnostic efficacy of T_1W&T_2WFS models was the best in both groups (all $p < 0.05$), and there was no significant difference between T_1W models and T_2WFS model (all $p > 0.05$) (Figure 3, Table 4).

DISCUSSION

Our study constructed the radiomics models of MR images that showed good diagnostic efficacy in assessing HF and inflammatory activity. The model of T_1W images was more effective than the model of T_2WFS images in diagnosing $F \geq 2$ of HF stage, which might be related to the extracted radiomic features. The gray-level co-occurrence matrix and gray-level run-length matrix are the most commonly used eigenvalues to reflect the radiographic maximum grayscale intensity that depends on the maximum grayscale intensity within the selected liver segment.[18] One study showed that iron deposition of different degrees could occur with HF development.[19] So, the decreased gray value of T_2WFS images might be the reason for the difference in the diagnostic efficacy. The similar result was found in previous studies.[20]

Hepatocyte injury-induced inflammation and HF can lead to changes in the water content and distribution ratio in the liver tissue. Factors, such as cell edema and an increased ratio of free water to bound water, could lead to increased T1 and T2 values.[21] Severe HF and cirrhosis can be diagnosed on conventional MR images due to significant reticular and nodular changes in liver texture. Conversely, it is difficult to diagnose less severe HF due to relatively mild texture changes, yet radiomics has the potential to quantitatively measure hepatic heterogeneity and captures subtle alterations. Though, several prior studies[22–24] have reported that texture analyses based on conventional T_1W and/or T_2WFS images have some diagnostic power for staging HF, these studies simply analyzed texture features on T_1W and T_2W images, and there was no analysis based on the combination of the two sequences. Therefore, our study may be the first, as far as we know, to explore models from T_1W images combined with T_2WFS images for staging fibrosis and grading inflammatory activity.

Previous studies have reported that the value of T1 and T2 were correlated with the pathological degree of liver fibrosis, and found that the T1 relaxation time/T2 relaxation time prolonged with the aggravation of liver fibrosis,[25,26] we found similar

Table 3. Performance of machine learning models in predicting fibrosis stage

	Radiomics label	AUC	95% CI	Sensitivity (%)	Specificity (%)	Delong Test
$F \geq 1$	T_1W	0.844	0.800–0.881	91.87	73.33	———
	T_2W	0.857	0.815–0.893	73.50	86.67	p^a=0.984
	T_1W&T_2W	0.932	0.899–0.957	78.80	97.78	$p^\dagger$<0.05, $p^\ddagger$<0.05
$F \geq 2$	T_1W	0.857	0.815–0.893	73.57	89.11	———
	T_2W	0.781	0.733–0.825	65.93	83.17	p^a<0.05
	T_1W&T_2WFS	0.915	0.880–0.913	85.46	93.07	$p^\dagger$<0.05, $p^\ddagger$<0.05

AUC, area under the curve; CI, confidence interval.
[a]:$p > 0.05$ compared to model built with T_1W ; [†]:$p < 0.05$ compared to model built with T_1W ; [‡]:$p < 0.05$ compared to model built with T_2W.

Table 4. Performance of machine learning models in predicting inflammatory activity grading

	Radiomics label	AUC	95% CI	Sensitivity (%)	Specificity (%)	Delong test
$A \geq 1$	T_1W	0.831	0.786–0.870	63.86	87.50	
	T_2W	0.854	0.811–0.890	75.36	85.33	p^a=0.541
	T_1W&T_2W	0.934	0.902–0.959	94.29	85.42	$p^\dagger$<0.05, $p^\ddagger$<0.05
$A \geq 2$	T_1W	0.838	0.794–0.877	91.94	64.10	
	T_2W	0.819	0.772–0.859	70.62	70.49	p^a=0.155
	T_1W&T_2W	0.910	0.873–0.938	79.83	91.45	$p^\dagger$<0.05, $p^\ddagger$<0.05

AUC, area under the curve; CI, confidence interval.
[a]:p > 0.05 compared to model built with T_1W ; [†]:p < 0.05 compared to model built with T_1W ; [‡]:p < 0.05 compared to model built with T_2W.

results in our study. Furthermore, Hiroki et al[27] found a weak correlation between the average gray value of T_2W images and the degree of liver fibrosis by both computer algorithm analysis and radiologist evaluation. We considered that the discrepancies between our findings and those of Hiroki et al might be due to different data processing methods and different sample sizes at each stage of liver fibrosis. In addition, the difference in magnetic field intensity could also, to a certain extent, affect the results. According to the previous literature,[28] the classification accuracy of 3.0 T MRI modalities was better than that of 1.5 T MRI in the classification of liver fibrosis.

In our study, the radiomics models constructed from T_1W, T_2WFS and T_1W&T_2WFS images could effectively diagnose fibrosis Stage 2. According to relevant study, the presence of significant fibrosis that referred to METAVIR score reaching F2, was a clear indicator of disease progression to end-stage liver disease.[2] For the patients whose HF stage is more than F2, additional therapy, besides symptomatic treatment, is required to realize the prevention of CLD. Therefore, early detection of significant fibrosis is important to making proper treatment decisions.

In most cases, chronic hepatitis precedes fibrosis. The persistence of chronic inflammation is closely related to the development of HF and cirrhosis.[29] Therefore, the evaluation of inflammatory activity is also very important. It has been reported that CLD patients with inflammatory activity A2 have a higher risk of cirrhosis.[30] Thus, accurate diagnosis of inflammatory activity A2 has important clinical significance. In this study, the radiomics models created based on T_1W, T_2WFS, and T_1W&T_2WFS images showed excellent diagnostic performance in detecting ≥A1/2 grades. Thus, we believe that radiomics models-based conventional MR images have the potential to diagnose and predict the grades of inflammatory activity.

As a simple iterative algorithm, the SGD classifier has been shown to be a very effective machine learning method, with the significant advantage of shortening the training time without affecting the accuracy of the model results and capable of effectively reducing training errors.[31,32] However, when the SGD classifier operates on large-scale problems, slow convergence and difficulty in regulation will occur, which requires further explore appropriate machine learning algorithms in depth in the future. In addition, because T_1W and T_2WFS images scans can be affected by a variety of factors, such as imaging parameters, hepatic iron concentration and fat content, future studies shall validate the suitability of the models and characterize these effects to improve model diagnostics efficacy.

LIMITATIONS

This study has some limitations. Firstly, our research was single center, which might lead to potentially biased results. External validation of the model in a larger multicenter cohort study should be required to demonstrate its robustness before being put into clinical practice. Secondly, the etiology of CLD was complicated, which included hepatitis C, hepatitis B, autoimmune hepatitis, non-alcoholic fatty liver disease and drug-induced hepatitis. Moreover, considering that too few patients in the F0/A0 group had liver biopsy, we included the normal number of cases in the F0/A0 group, which might lead to some bias in the results. Finally, the ROI selected was a local range at the level of right hepatic portal vein, avoiding large blood vessels and bile ducts. However, due to the heterogeneity of HF, the choice of ROI might affect models test performance. We will further test the potential influence of ROI selection in the future.

CONCLUSION

Radiomics models built on conventional non-contrast MRI scans can be used for predicting the stages of liver fibrosis and the grades of inflammatory activity. The models built on combining both sequences may have better diagnostic performance than those built on T_1W or T_2WFS images alone.

CONFLICT OF INTEREST

All authors declare that they have no conflicts of interest.

REFERENCES

1. Hytiroglou P, Theise ND. Regression of human cirrhosis: an update, 18 years after the pioneering article by wanless et al. *Virchows*

Arch 2018; **473**: 15–22. https://doi.org/10.1007/s00428-018-2340-2
2. Parola M, Pinzani M. Liver fibrosis: pathophysiology, pathogenetic targets and clinical issues. *Mol Aspects Med* 2019; **65**: S0098-2997(18)30070-0: 37–55: . https://doi.org/10.1016/j.mam.2018.09.002
3. Regev A, Berho M, Jeffers LJ, Milikowski C, Molina EG, Pyrsopoulos NT, et al. Sampling error and intraobserver variation in liver biopsy in patients with chronic HCV infection. *Am J Gastroenterol* 2002; **97**: 2614–18. https://doi.org/10.1111/j.1572-0241.2002.06038.x
4. Wong JB, Bennett WG, Koff RS, Pauker SG. Pretreatment evaluation of chronic hepatitis C: risks, benefits, and costs. *JAMA* 1998; **280**: 2088–93. https://doi.org/10.1001/jama.280.24.2088
5. Taouli B, Ehman RL, Reeder SB. Advanced MRI methods for assessment of chronic liver disease. *AJR Am J Roentgenol* 2009; **193**: 14–27. https://doi.org/10.2214/AJR.09.2601
6. Zheng Y, Xu Y-S, Liu Z, Liu H-F, Zhai Y-N, Mao X-R, et al. Whole-liver apparent diffusion coefficient histogram analysis for the diagnosis and staging of liver fibrosis. *J Magn Reson Imaging* 2020; **51**: 1745–54. https://doi.org/10.1002/jmri.26987
7. Fu F, Li X, Liu Q, Chen C, Bai Y, Shi D, et al. Noninvasive DW-MRI metrics for staging hepatic fibrosis and grading inflammatory activity in patients with chronic hepatitis B. *Abdom Radiol (NY)* 2021; **46**: 1864–75. https://doi.org/10.1007/s00261-020-02801-2
8. Bülow R, Mensel B, Meffert P, Hernando D, Evert M, Kühn JP. Diffusion-Weighted magnetic resonance imaging for staging liver fibrosis is less reliable in the presence of fat and iron. *Eur Radiol* 2013; **23**: 1281–87. https://doi.org/10.1007/s00330-012-2700-2
9. Huwart L, Sempoux C, Vicaut E, Salameh N, Annet L, Danse E, et al. Magnetic resonance elastography for the noninvasive staging of liver fibrosis. *Gastroenterology* 2008; **135**: 32–40. https://doi.org/10.1053/j.gastro.2008.03.076
10. Rouvière O, Yin M, Dresner MA, Rossman PJ, Burgart LJ, Fidler JL, et al. Mr elastography of the liver: preliminary results. *Radiology* 2006; **240**: 440–48. https://doi.org/10.1148/radiol.2402050606
11. Hoodeshenas S, Yin M, Venkatesh SK. Magnetic resonance elastography of liver: current update. *Top Magn Reson Imaging* 2018; **27**: 319–33. https://doi.org/10.1097/RMR.0000000000000177
12. Lambin P, Rios-Velazquez E, Leijenaar R, Carvalho S, van Stiphout RGPM, Granton P, et al. Radiomics: extracting more information from medical images using advanced feature analysis. *Eur J Cancer* 2012; **48**: 441–46. https://doi.org/10.1016/j.ejca.2011.11.036
13. Gillies RJ, Kinahan PE, Hricak H. Radiomics: images are more than pictures, they are data. *Radiology* 2016; **278**: 563–77. https://doi.org/10.1148/radiol.2015151169
14. Bedossa P, Poynard T. An algorithm for the grading of activity in chronic hepatitis C. *Hepatology* 1996; **24**: 289–93. https://doi.org/10.1002/hep.510240201
15. Bahl G, Cruite I, Wolfson T, Gamst AC, Collins JM, Chavez AD, et al. Noninvasive classification of hepatic fibrosis based on texture parameters from double contrast-enhanced magnetic resonance images. *J Magn Reson Imaging* 2012; **36**: 1154–61. https://doi.org/10.1002/jmri.23759
16. DeLong ER, DeLong DM, Clarke-Pearson DL. Comparing the areas under two or more correlated receiver operating characteristic curves: a nonparametric approach. *Biometrics* 1988; **44**: 837–45. https://doi.org/10.2307/2531595
17. Moons KGM, Altman DG, Reitsma JB, Ioannidis JPA, Macaskill P, Steyerberg EW, et al. Transparent reporting of a multivariable prediction model for individual prognosis or diagnosis (TRIPOD): explanation and elaboration. *Ann Intern Med* 2015; **162**: W1–73. https://doi.org/10.7326/M14-0698
18. van Griethuysen JJM, Fedorov A, Parmar C, Hosny A, Aucoin N, Narayan V, et al. Computational radiomics system to decode the radiographic phenotype. *Cancer Res* 2017; **77**: e104–7. https://doi.org/10.1158/0008-5472.CAN-17-0339
19. Metwally MA, Zein CO, Zein NN. Clinical significance of hepatic iron deposition and serum iron values in patients with chronic hepatitis C infection. *Am J Gastroenterol* 2004; **99**: 286–91. https://doi.org/10.1111/j.1572-0241.2004.04049.x
20. Schawkat K, Ciritsis A, von Ulmenstein S, Honcharova-Biletska H, Jüngst C, Weber A, et al. Diagnostic accuracy of texture analysis and machine learning for quantification of liver fibrosis in MRI: correlation with Mr elastography and histopathology. *Eur Radiol* 2020; **30**: 4675–85. https://doi.org/10.1007/s00330-020-06831-8
21. Chow AM, Gao DS, Fan SJ, Qiao Z, Lee FY, Yang J, et al. Measurement of liver T_1 and T_2 relaxation times in an experimental mouse model of liver fibrosis. *J Magn Reson Imaging* 2012; **36**: 152–58. https://doi.org/10.1002/jmri.23606
22. Zhao R, Gong X-J, Ge Y-Q, Zhao H, Wang L-S, Yu H-Z, et al. Use of texture analysis on noncontrast MRI in classification of early stage of liver fibrosis. *Can J Gastroenterol Hepatol* 2021; **2021**: 6677821. https://doi.org/10.1155/2021/6677821
23. Cannella R, Borhani AA, Tublin M, Behari J, Furlan A. Diagnostic value of MR-based texture analysis for the assessment of hepatic fibrosis in patients with nonalcoholic fatty liver disease (NAFLD). *Abdom Radiol (NY)* 2019; **44**: 1816–24. https://doi.org/10.1007/s00261-019-01931-6
24. House MJ, Bangma SJ, Thomas M, Gan EK, Ayonrinde OT, Adams LA, et al. Texture-based classification of liver fibrosis using MRI. *J Magn Reson Imaging* 2015; **41**: 322–28. https://doi.org/10.1002/jmri.24536
25. Kreft B, Dombrowski F, Block W, Bachmann R, Pfeifer U, Schild H. Evaluation of different models of experimentally induced liver cirrhosis for MRI research with correlation to histopathologic findings. *Invest Radiol* 1999; **34**: 360–66. https://doi.org/10.1097/00004424-199905000-00006
26. Thomsen C, Christoffersen P, Henriksen O, Juhl E. Prolonged T1 in patients with liver cirrhosis: an in vivo MRI study. *Magn Reson Imaging* 1990; **8**: 599–604. https://doi.org/10.1016/0730-725x(90)90137-q
27. Kato H, Kanematsu M, Zhang X, Saio M, Kondo H, Goshima S, et al. Computer-Aided diagnosis of hepatic fibrosis: preliminary evaluation of MRI texture analysis using the finite difference method and an artificial neural network. *AJR Am J Roentgenol* 2007; **189**: 117–22. https://doi.org/10.2214/AJR.07.2070
28. Zhang X, Gao X, Liu BJ, Ma K, Yan W, Liling L, et al. Effective staging of fibrosis by the selected texture features of liver: which one is better, CT or MR imaging? *Comput Med Imaging Graph* 2015; **46 Pt 2**: S0895-6111(15)00125-1: 227–36: . https://doi.org/10.1016/j.compmedimag.2015.09.003
29. Czaja AJ, Carpenter HA. Progressive fibrosis during corticosteroid therapy of autoimmune hepatitis. *Hepatology* 2004; **39**: 1631–38. https://doi.org/10.1002/hep.20235
30. Tang CM, Yau TO, Yu J. Management of chronic hepatitis B infection: current treatment guidelines, challenges, and new developments. *World J Gastroenterol* 2014; **20**: 6262–78. https://doi.org/10.3748/wjg.v20.i20.6262
31. Wikipedia_SGD. Stochastic gradient descent. 2013. Available from: http://en.wikipedia.org/wiki/Stochastic_gradient_descent#cite_ref-6
32. Zhang W, Zhang L, Jin Z, Jin R, Cai D, Li X, et al. Sparse learning with stochastic composite optimization. *IEEE Trans Pattern Anal Mach Intell* 2017; **39**: 1223–36. https://doi.org/10.1109/TPAMI.2016.2578323